THE MICROSTRUCTURAL DEVELOPMENT OF TYPE 321 AUSTENITIC STAINLESS STEEL WITH LONG TERM AGEING

Dr Rebecca Higginson[1], Mr Graham Green[1], Dr Simon Hogg[1], Dr Sarah Spindler[2], Dr Christopher Hamm[2]

Abstract

Austenitic stainless steel is important in the power generation industry where it is expected to be in service at high temperatures for extended periods of time. Work carried out on the microstructural development of two 321 stainless steel samples has shown that there are complex phase changes that can take place in this alloy. Although the alloy is expected to be fully austenitic at room temperature there is a fraction of ferrite present in the as-received materials. High temperature XRD has shown that this ferrite phase can be dissolved at temperatures between 800 and 900°C but precipitates on cooling at temperatures below 200°C. Due to the low temperature of formation, similarities in chemistry and orientations relationships indicate that the ferrite is forming in a displacive manor from the austenite grains. Thermal ageing at 750°C has been carried out up to times of 15,000 hours and the microstructural changes quantified. The fraction of sigma phase and ferrite increases with ageing time with a corresponding decrease in austenite fraction. This change in the microstructure is postulated to be caused by the changes in the matrix chemistry due to the formation of second phases particles.

Keywords: Stainless Steel, Long Term Ageing, Phase Development, Sigma Phase

1. Introduction

Austenitic stainless steels are extensively used in the power generation industry for high temperature applications due to their excellent mechanical and oxidation properties [1]. In the power generation industry, these alloys need to maintain their properties over extended periods of time at elevated temperatures. However, the exposure of highly alloyed steels to high temperature can cause changes in the microstructure to occur, particularly in terms of second phase particles that form as the metal transforms towards its equilibrium condition. In the 300 series stainless steel alloys these second phases include chromium rich carbides, for example $M_{23}C_6$ where M is a chromium rich combination of metallic elements, and intermetallics such as sigma phase [2]. Sigma phase, in particular, can influence the mechanical properties of the bulk metal as it is a brittle phase that can form in large quantities, and so an understanding of the microstructural development is critical for allowing accurate prediction of the viable lifetimes of components. Hsieh and Wu found that sigma phase formation in austenitic stainless steels can occur at between 600°C and 1000°C and can take many thousands of hours to form [2]. Recent work by the authors found that the formation of

[1] Department of Materials, Loughborough University, Loughborough, Leicestershire, LE11 3TU, UK

[2] EDF Energy, Barnett Way, Barnwood, Gloucestershire, GL4 3RS, UK

sigma phase is significantly enhanced if stabilising elements, such as titanium are used, or if delta ferrite is present [3].

For high temperature applications, grades of stainless steel have been developed which contain small additions of vanadium, titanium and niobium which improve the mechanical properties and the resistance to stress corrosion cracking. One of these alloys is Type 321 (1.4521 or S32100) stainless steel which contains an addition of titanium. The titanium forms titanium carbo-nitrides that inhibit the formation of chromium carbides and as such reduce the sensitisation potential of the alloy. Over extended period of time at operating temperatures, however, the initial microstructure changes as the material moves towards its equilibrium state. The main second phase that is known to form in these alloys is sigma phase. Guan *et al.* investigated the effect of thermal ageing at 700°C for times of up to 6,000 hours on 321 and 347 grades [4]. They found that TiN and NbN initially form followed by a small amount of $M_{23}C_6$ then sigma phase. The presence of the stabilising elements is thought to promote sigma phase formation as the formation of $M_{23}C_6$ is retarded, and as such, leaves chromium free to form sigma phase. This is illustrated as a 321 grade stainless steel can form sigma phase in less than 100 hours of ageing at 750°C [3]. This can be contrasted to a standard 316 grade austenitic stainless steel which does not contain stabilising elements, and as such forms chromium carbides after a few hour hours at 750°C but does not form sigma phase for ~2000 hours at 750°C [5].

Recent work by the authors [6] has shown that the ageing of parent and weld metals of a 321 grade stainless steel tube is complex with the formation of a ferrite phase during ageing. The ferrite phase was found to form with a displacive manner from the austenite with little detectable change in the chemistry of the metal in the differing phases. The composition of the steels was analysed using a DeLong diagram [7], where it was theorised that the low nitrogen content was the cause of the low temperature transformation of austenite to ferrite. The low nitrogen content is important as it is known to be a strong austenite promoting element [8]. It was also suggested that the formation of sigma phase during thermal ageing was the cause of the reduction in austenite stability with ageing time. This effect has not been reported previously in this alloy system, with the alloy expected to remain austenitic even after longer times at temperature. This paper considers the formation of ferrite in two 321 alloys with differing starting structures after extended periods of ageing with detailed quantification of the microstructures.

2. Experimental Procedure

The material was received in thin section tube material (4mm thick) or as a thick plate (~25mm thick). The as-received chemical compositions of the two materials are given in Table 1. These compositions were used for thermodynamic predication of the phases at equilibrium using Thermo-Calc software package using the TCFE5 database for steels.

Sections of the materials were taken for long term heat treatment and encapsulated in quartz tubes which had been back filled with argon to prevent oxidation during the exposure. These were heat treated in a box furnace for times up to 15,000 hour at a temperatures of 750°C to allow accelerated ageing of the material. Following heat treatment, the samples were removed from the furnace and allowed to cool before being removed from the tubes.

Samples were mounted in conductive Bakelite and prepared metallographically using standard grinding and polishing techniques that finish on either 1μm diamond or colloidal silica polish for ~20 minutes for examination using Electron Backscatter Diffraction (EBSD).

The prepared samples were examined using optical microscopy or a LEO 1530VP Field Emission Gun Scanning Electron Microscope (FEGSEM) with is equipped with an EBSD system with chemical information gathered using Energy Dispersive X-ray Spectroscopy (EDS).

A Nova Nanolab 600 dualbeam FIBSEM system was used study the second phase particles without having to use chemical etchants. The charged gallium atom ion beam was used to produce secondary electron images of the surfaces as it gave excellent contract between the matrix and the second phase particles. The images were analysed using image analysis software and the particles size and volume fractions determined.

High temperature X-ray diffraction was carried out in a GeniX high flux X-ray system with FOX 2D 10_30P mirror, which had a 230μm beam of Cu K alpha radiation. Samples of the material were cut to 10x5mm strips and the surface prepared by mechanical grinding to ~100μm in thickness and finally polished to a mirror finish. The X-ray system was in a vacuum chamber and the air evacuated to prevent oxidation during the testing. A thermocouple was used to monitor the temperature during the test. The sample was heated in increments to 1000°C and data collected at the hold temperatures over a 5 minute period on both the heating and cooling cycle.

Table 1: Chemical composition of the two alloys used in the study (wt %) balance Fe

	C	Si	Mn	P	S	Cr	Mo	Ni
Thin Section	0.046	0.56	1.53	0.019	0.01	17.38	0.45	8.92
Thick Section	0.06	0.45	1.82	0.025	0.001	17.12	0.33	9.34

	Ti	Cu	Al	Nb	Co	W	V	N
Thin Section	0.33	<0.01	0.046	0.02	0.05	0.11	–	–
Thick Section	0.34	0.27	0.049	<0.01	–	–	0.06	0.015

3. Results and Discussion

Type 321 stainless steel should be predominately austenitic a room temperature. Examination of the as received material however showed there was a proportion of a BCC phase present in the structure of both the thin wall tube and thick section. Figure 1 shows EBSD scans of the as received materials showing inverse pole figure maps and the corresponding phase maps. There is a difference in the grain size of the two materials with the thin section showing a small more homogeneous grain size distribution (~10μm), Figure 1(a). The thicker section 321 material, shown in Figure 1(c), has a larger grain size (~60μm) with some larger grains seen in the material,. The thin section shows some directionality in the structure probably due to the rolling of the sheet from which the tube was formed. The

phase maps show that although the majority of the structure is FCC austenite there are a large number of regions that are indexed as BCC ferrite. Thermodynamic equilibrium calculations using Thermocalc showed that both materials were predicted to contain a fraction of ferrite at room temperature with structure being ~100% austenitic at ~770°C. The equilibrium structure is also predicted to contain a high fraction of sigma phase, carbides and a number of other intermetallic phases [3,6].

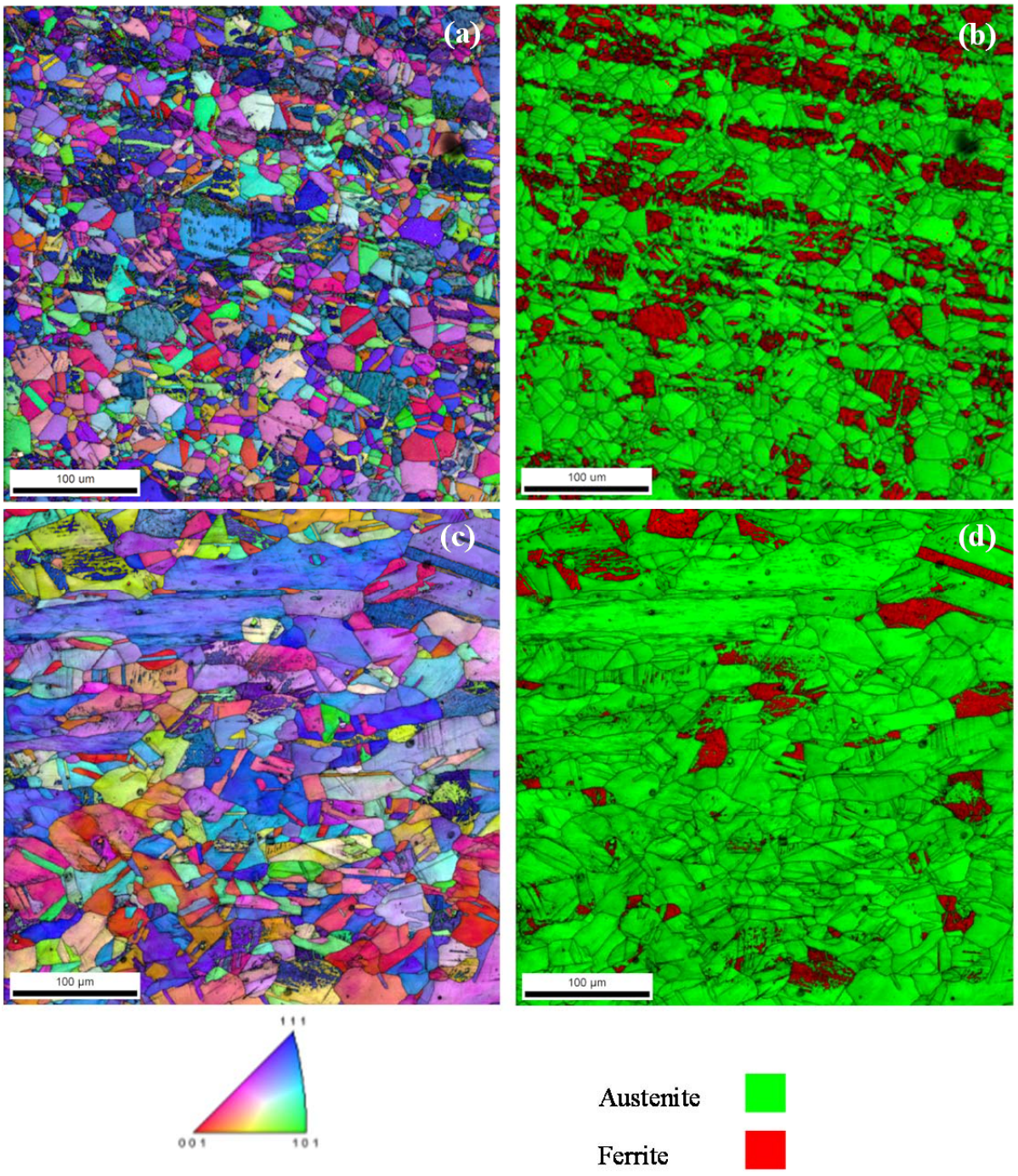

Figure 1: Electron Backscatter direction maps of the as received materials (a) in inverse pole figure map of the thin section with (b) the corresponding phase map and (c) the inverse pole figure map of the thick section materials with (d) the corresponding phase map.

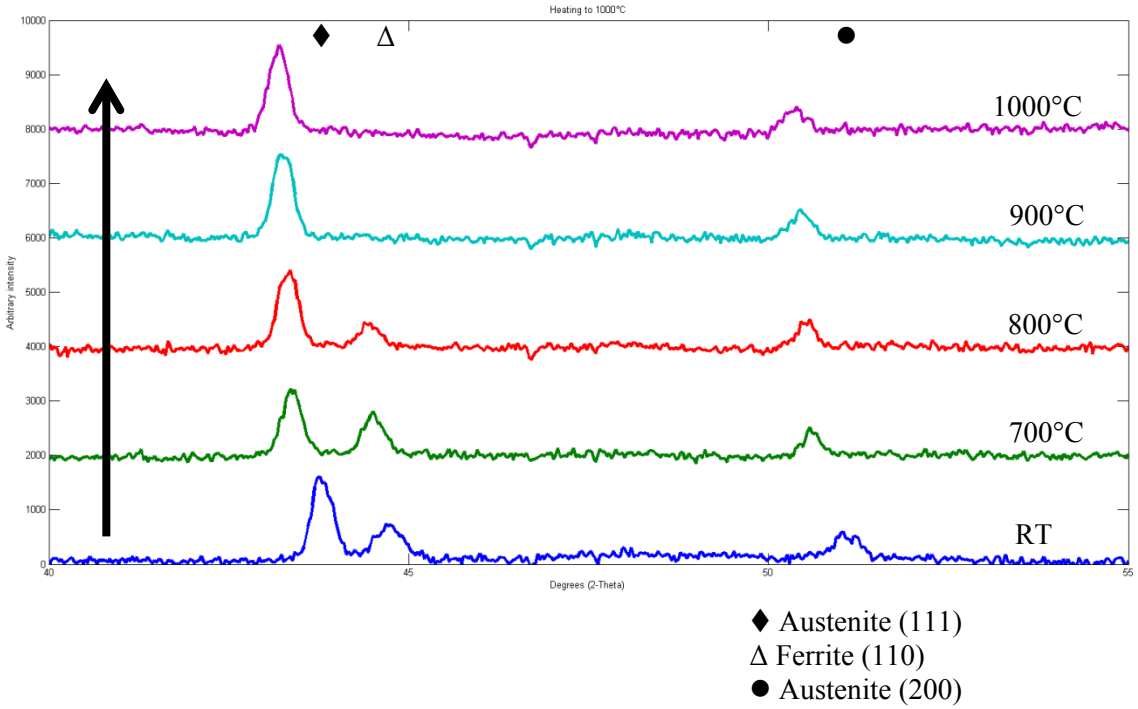

Figure 2: High temperature XRD traces for the thin section materials heating to 1000°C (the traces have been offset by 2000 to allow comparisons to be made)

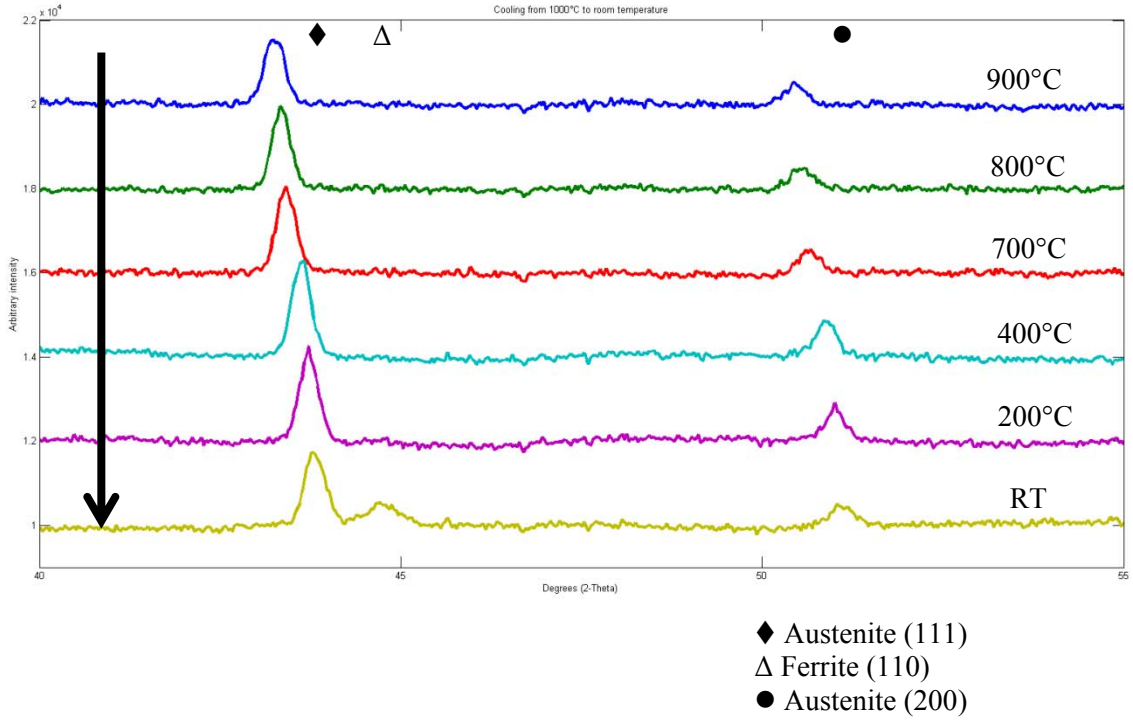

Figure 3: High temperature XRD traces for the thin section materials cooling to temperatures from 1000°C (see Fig.2) to room temperature (the traces have been offset by 2000 to allow comparisons to be made)

Figure 2 shows XRD data collected from the thin sections materials as it is heated to 1000°C. At room temperature the structure shows peaks for both FCC austenite and BCC ferrite. As the temperature increases both phases appear to be stable until between 800 and 900°C where the structure becomes 100% austenite. This fits to some extent the thermodynamic calculations where 100% austenite is predicted above 770°C the discrepancy may be the time it takes for the full transformation to take place. At 1000°C the sample is shown to be 100% austenite. Figure 3 shows the XRD data taken on cooling the samples back to room temperature. The material remained 100% austenite until a temperature between 200°C and above room temperature with the BCC peak being slightly lower than that at the start of the experiment. The low temperature at which the phase change takes place suggests that the transformation from austenite to ferrite is displacive. EDSD/EDS data in weld metal of similar composition has shown that the new ferrite phase that forms has a similar chemistry and orientation to the austenite grains in which it forms [8].

The thermodynamic calculations are a prediction of the material phases at equilibrium. To determine how the metal changes with time, long term heat treatment were carried out at 750°C for times up to 15,000 hours. Following heat treatment the samples were prepared and analysed with EBSD and EDS to quantify the changes in the microstructure. As the main phases that were predicted thermodynamically were ferrite, austenite and sigma, these were quantified on a number of micrographs and the results are plotted in the Figure 4 for the thin section and Figure 5 for the thick section samples. The initial microstructure shows that the thin section is ~80% austenite and 20% ferrite whereas the thick section is over 90% austenite. As the time at temperature increases, the fraction of austenite decreases as the ferrite increases. The sigma phase also increases with time with more seen in the thick section materials at a given time.

Figure 6 shows a typical low magnification EBSD phase map after heat treatment at 750°C for the maximum time studied of 15,000hours. In this area the structure is shown to be predominantly ferrite (red phase) with austenite plotted as green. Within the ferrite grains there is internal structure visible which is lath like in nature, this internal structure is not as evident in the ferrite in the as-received materials, shown in Figure 1. Figure 7 shows a higher magnification scan of the area highlighted in Figure 6. The image quality map and the inverse pole figure map clearly show the internal structure within the ferrite grains (Figure 7 (b) and (c) respectively), although the amount of lattice rotation within individual grains varies. The sigma phase is clearly visible in the microstructure, shown as blue in Figure 7(a). The EDS maps of the same area, shown in Figures 7(d-g), highlight that the sigma phase is richer in chromium and manganese and depleted in iron and nickel compared to the surrounding matrix. There is no detectable difference in the chemistry of the ferrite and austenite phases however the technique cannot detect light elements, for example carbon and nitrogen which may be significant in the development of the microstructure [3,6].

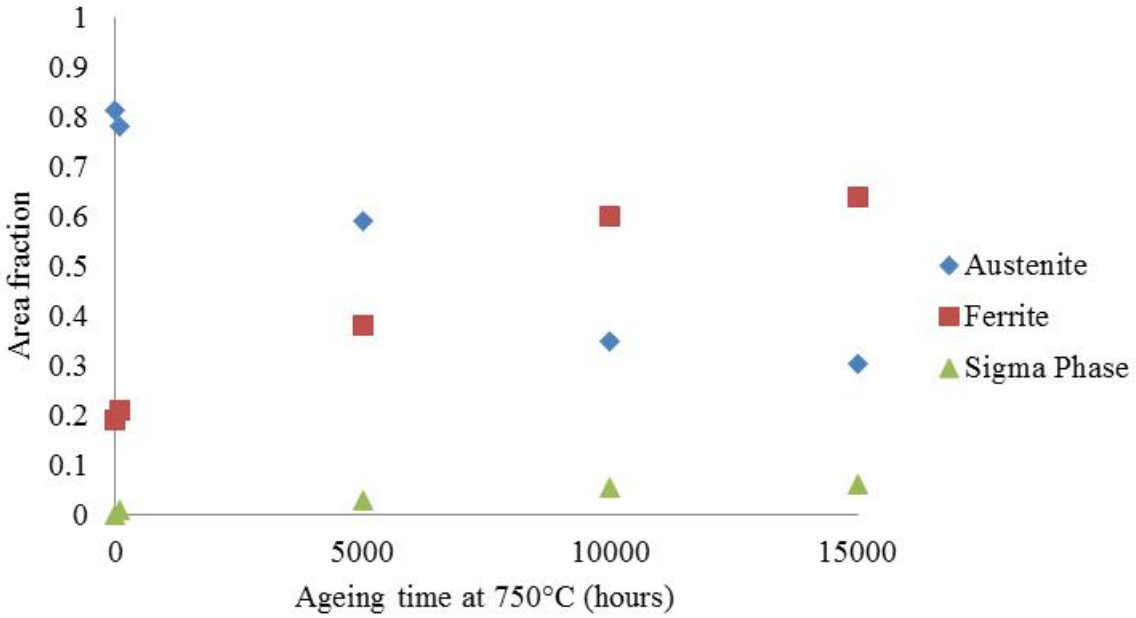

Figure 4: Fraction of phases measured in the thin section with ageing time at 750°C measured by EBSD analysis.

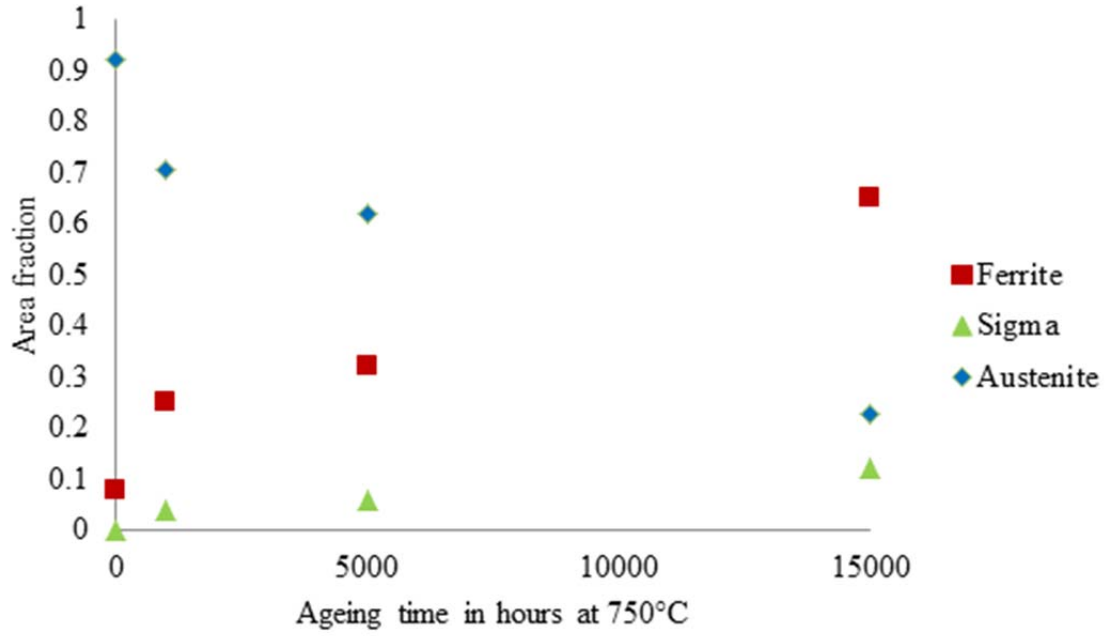

Figure 5: Fraction of phases measured in the thick section with ageing time at 750°C measured by EBSD analysis.

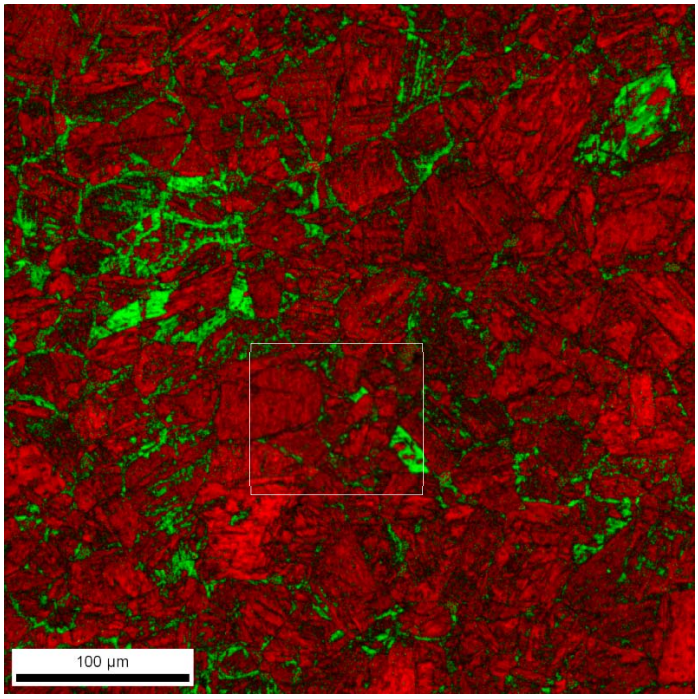

Phase	Colour
Austenite	
Ferrite	
Sigma	

Figure 6: EBSD phase map of the thick section material following ageing at 750°C for 15,000 hours.

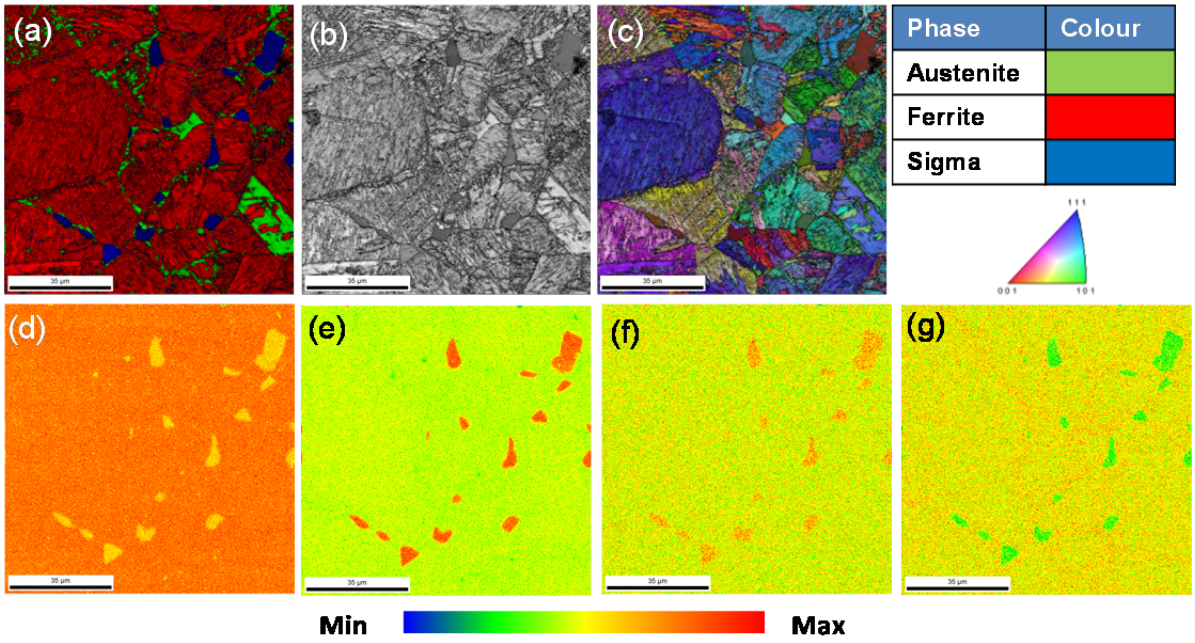

Figure 7: High resolution EBSD and EDX maps of the section marked in Figure 6. Figure 7(a) shows the phase map, (b) the image quality map, (c) the orientation map, (d) the iron map (e) the chromium map (f) the manganese map and (g) the nickel map.

Figure 8 shows a plot of the particle size and area fraction of the thin section aged at 750°C for times up to 15,000 hours. The measurements were taken using ion induced secondary

electron imaging which gives excellent contrast between the matrix and the second phase. The particle size is given as equivalent round diameter. The area fraction increases up to a time between 2,000 and 8,000 hours and then levels out. As the time increases the errors in the data a slightly bigger and so whether the data slightly decreases is difficult to conclude. The particle size gradually increases with a large increase between 12,000 and 15,000 hours where there is an increase in particle size probably due to the growth of larger particles at the expense of smaller ones.

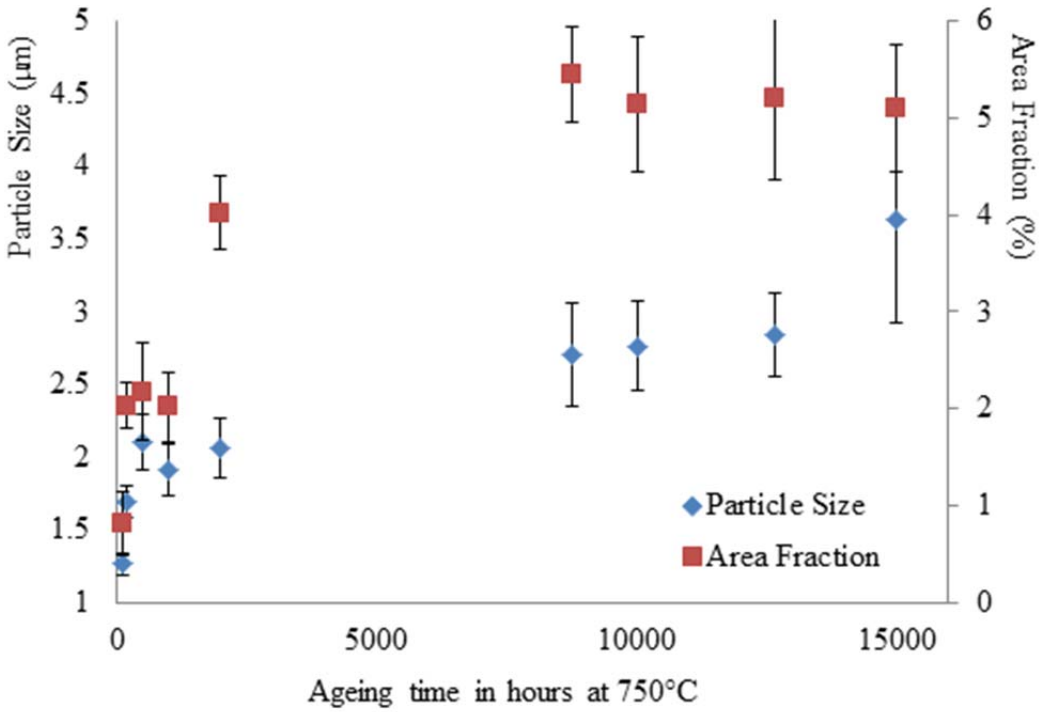

Figure 8: Quantification of the particle size and area fraction of the thin section material measured using ion induced secondary electron imaging of the material aged at 750°C for times up to 15,000 hours.

The formation of sigma phase is well documented although here are differences between the results in the literature in the time it takes for sigma to form. This may be due to differences in the initial microstructure and chemistry. The increase in ferrite phase is more difficult to explain particularly as it has not been reported in the literature. There may be a number of reasons for this including the fact that as it not expected to form in these alloys it has not been scrutinised if it was in the material. This is also true for EBSD where the expected phases need to be input into the system before a scan is carried out. It is also difficult to differentiate between ferrite and martensitic using EBSD. The substructure visible in Figure 7 does look like the lath like structure of martensite. The authors have postulated that changes in the chemistry of the material during ageing, particularly in terms of light elements may lead to the formation of martensite in this alloy [6]. Further work is needed however to prove this theory.

4. Conclusions

Two different samples of Type 321 stainless steel have been examined in terms of their starting microstructure and its development during long term ageing. The as received microstructure shows a high proposition of a ferrite phase. High temperature XRD has shown that this is stable up to temperatures above 800°C where the structure becomes 100% austenite. On cooling the material remains austenite to ~200°C where the ferrite phase reforms. Quantification of the microstructure during ageing has demonstrated that there is an increase in the ferrite phase, at the expense of austenite, as the ageing time increases. The fraction of sigma phase also increases in both alloys. Particle analysis has shown that there is initially a rapid increase in sigma phase followed by a long period where there is little change in the size or volume fraction. At 15,000 hours, however, there may be a slight further increase in particle size although longer time data would be needed to confirm this. It is postulated that the phase change from austenite to ferrite is linked to the formation of the second phases as they may reduce the amount of austenite stabilising elements in the bulk material.

5. References

[1] W. J. MILLS, "Heat-to-heat variations in the fracture toughness of austenitic stainless steels," Eng Fract Mech, 30 (5) pp 469-492, 1988

[2] C. C. Hsieh and W. Wu, "Overview of Intermetallic Sigma Phase Precipitation in Stainless Steels," ISRN Metallurgy, 2012

[3] G. Green; R. Higginson; S. Hogg; S. Spindler; C. Hamm "Evolution of sigma phase in 321 grade austenitic stainless steel parent and weld metal with duplex microstructure" Mater Sci Tech, 30(12), pp. 1392-1398, 2013

[4] K. Guan, X. Xiadong and Z. Wang, "Effect of aging at 700 °C on precipitation and toughness of AISI 321 and AISI 347 austenitic stainless steel welds," Nucl Eng Des, 235, pp.2485-2494, 2005

[5] B. Weiss and R. Stickler, "Phase instabilities during high temperature exposure of 316 austenitic stainless steel," Metal. Trans., 3, pp. 851-866, 1972

[6] G. Green, R. Higginson, S. Hogg, S. Spindler, C. Hamm, J. Najorka "Analysis of ferrite formed in 321 grade austenitic stainless steel" Mater Sci Tech31 (4), pp. 418-425, 2015

[7] W. Delong, "A modified phase diagram for stainless steel weld metals", Met. Prog, p. 98, 1960

[8] V. Raghavan and D. Antia, "The chromium equivalents of selected elements in austenitic stainless steels," Metall Mat Trans A, 25, pp. 2675-2681, 1994